J Electr Eng Technol.2018; 13(3): 1241-1250
http://doi.org/10.5370/JEET.2018.13.3.1241

ISSN(Print) 1975-0102
ISSN(Online) 2093-7423

Model Predictive Control of Circulating Current Suppression in Parallel-Connected Inverter-fed Motor Drive Systems

Shin-Won Kang*, Jae-Hwan Soh* and Rae-Young Kim†

Abstract – Parallel three-phase voltage source inverters in a direct connection configuration are widely used to increase system power ratings. A zero-sequence circulating current can be generated according to the switching method; however, the zero-sequence circulating current not only distorts current, but also reduces the system reliability and efficiency. In this paper, a model predictive control scheme is proposed for parallel inverters to drive an interior permanent magnet synchronous motor with zero-sequence circulating current suppression. The voltage vector of the parallel inverters is derived to predict and control the torque and stator flux components. In addition, the zero-sequence circulating current is suppressed by designing the cost function without an additional current sensor and high-impedance inductor. Simulation and experimental results are presented to verify the proposed control scheme.

Keywords: Parallel three-phase voltage source inverters, Zero-sequence circulating current, Interior permanent magnet synchronous motor(IPMSM), Model predictive control(MPC).

1. Introduction

The parallel connection of three-phase power converters is an effective method to enhance the power and reliability of the system. The use of standardized power converters has the additional advantage of reducing manufacturing costs; however, a zero-sequence circulating current occurs when a three-phase power converter is connected in parallel. The zero-sequence circulating current distorts the current and reduces the reliability and efficiency of the system. Many studies have been carried out on the suppression of zero-sequence circulating current in parallel inverters systems [1-9].

A simple solution to suppress circulating current in a parallel inverter system is the use of a separate AC or DC power supply, or an isolation transformer on the AC side. Although this technique is easy to apply, it has the disadvantage of increasing the volume and cost of the entire system due to the use of additional power sources or transformers. To overcome this drawback, the addition of a high impedance reactor has been proposed to provide a high zero-sequence impedance [1, 2]. While this method can prevent increases in both the volume and price of the system, the circulating current of the low frequency is not sufficiently suppressed.

Parallel power converters are generally connected directly to the AC and DC sides of two rectifiers or inverters through inverter control, without the use of additional components [3]. Since the inverter is directly connected, a circulating current may occur between the power converters in accordance with the control method. Also, in this case, since the sum of the three-phase inductor currents of each inverter output is not always zero, three-phase current sensing of the output inductor is needed to control the circulating current. Therefore, it is necessary to control the inverter to avoid generating circulating current in the direct connection method [4-6].

Many attempts have been made to apply the model predictive control (MPC) technique to power electronics systems due to the rapid and robust development of microprocessor technology in recent years [10-17]. MPC, which selects the optimal vector based on the cost function and includes a dynamic model of the system and the control variable, is easy to implement and has a fast dynamic response. MPC can be applied effectively to motor drives because it is suitable for non-linear and multivariable systems. Another reason to apply MPC to power electronics such as power converters and motor drives, is that one can take advantage of the inherent characteristics of power converters. Since the power converter has a limited number of switching states, the MPC optimization problem can be simplified to predict system operation for possible switching states.

When MPC is used for motor drives in a single inverter system, a cost function related to the errors of the magnetic flux and torque components is defined, and a vector minimizing this cost function is applied to the inverter [11]. However, if the current control is performed using the cost function of [11] in a parallel inverter system, a current imbalance may occur between the inverters depending on the switching state, and the output inductor currents may diverge. The conventional method to suppress circulating

† Corresponding Author: Dept. of Electrical and Biomedical Engineering, Hanyang University, Korea. (rykim@hanyang.ac.kr)
* Dept. of Electrical Engineering, Hanyang University, Korea. ({ksw117, jhsoh}@hanyang.ac.kr)
Received: September 20, 2017; Accepted: January 16, 2018

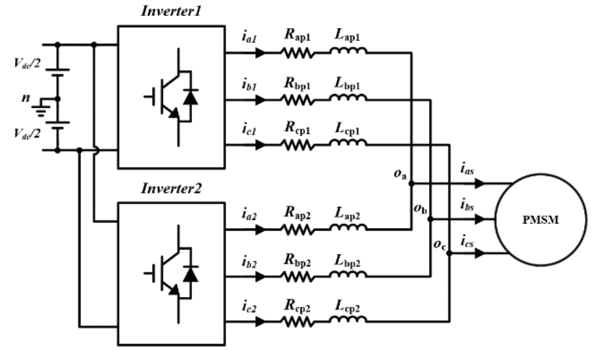

Fig. 1 Parallel-connected inverter-fed motor drive system

current in parallel inverter systems requires an additional current sensor to sense the current information of each output inductor [4-6]. While this allows for accurate control of the circulating current, both the volume and cost of the system are increased. Therefore, in this paper, we propose a circulating current suppression method using MPC in a parallel inverter-fed motor drive system, directly connected to the AC and DC side, without an additional current sensor or high-impedance inductor. The phase voltage, offset voltage, and output inductor voltage of the parallel inverters, including the motor, are modeled for parallel inverters and circulating current control. In order to suppress the circulating current in the MPC-based parallel inverter system, the appropriate voltage vector was applied to the inverters by adding the output inductor voltage term to the cost function using the predicted values of these voltages.

This paper is organized as follows: The basic structure of a parallel inverter system including a motor is described, and a method of modeling a voltage vector of a parallel inverter is explained in Section 2. The cost function of the MPC, used to suppress the circulating current using the model of the parallel inverters, is outlined in Section 3. In section 4, simulations and experimental results are presented to demonstrate the validity of the proposed method. Finally, the conclusion is summarized in Section 5.

2. System Model

2.1 System configuration

Fig. 1 shows the motor drive system using parallel three-phase voltage source inverters. The system consists of two voltage source inverters, output inductors and an interior permanent magnet synchronous motor (IPMSM). The AC output terminals of the two voltage source inverters are connected directly in parallel through the output inductors. As shown in Fig. 1, the three phases are represented by a, b, and c, respectively. The output inductor and equivalent resistance are connected to each phase, and the symbols are represented by L_{ipx} and R_{ipx}, respectively. Here, i represents the corresponding phase of the inverter and x represents the inverter number. Also, the nodes commonly connected to each output inductors and the motors are denoted by o_i, respectively. In Fig. 1, n represents the virtual neutral point of the DC-link and the a-phase AC current, which is the sum of the a-phase currents of Inverter 1 and Inverter 2, and is indicated by i_{as}. Similarly, the ac side currents of b-phase and c-phase are indicated by i_{bs} and i_{cs}, respectively. The current flowing in the output inductor of each inverter is represented by i_{ix}.

2.2 Modeling of PMSM

The stator voltage equation of a permanent magnet synchronous motor viewed from the stationary reference frame is as follows:

$$\vec{\boldsymbol{v}}_s = R_s \vec{\boldsymbol{i}}_s + \frac{d\vec{\boldsymbol{\lambda}}_s}{dt}, \tag{1}$$

where $\vec{\boldsymbol{v}}_s$ is the stator voltage, $\vec{\boldsymbol{i}}_s$ is the stator current, $\vec{\boldsymbol{\lambda}}_s$ is the magnetic flux, and R_s is the stator resistance. The stator flux linkage $\vec{\boldsymbol{\lambda}}_s$ is generated by the rotor magnet and the self-linked flux produced by the stator currents. This relation is described by

$$\vec{\boldsymbol{\lambda}}_s = L_s \vec{\boldsymbol{i}}_s + \psi_m e^{j\theta_r}, \tag{2}$$

where L_s is the stator self-inductance, ψ_m is the flux magnitude of the rotor magnet, and θ_r is the rotor position. By substituting (2) into (1), (3) can be obtained.

$$\vec{\boldsymbol{v}}_s = R_s \vec{\boldsymbol{i}}_s + L_s \frac{d\vec{\boldsymbol{i}}_s}{dt} + j\psi_m \omega_r e^{j\theta_r}, \tag{3}$$

where $\omega_r = d\theta_r / dt$ is the rotor speed.

Multiplying by $e^{-j\theta_r}$ and considering the stator voltage and current space vectors in the rotor reference frame aligned with the rotor flux axis, (3) can be represented by

$$\vec{\boldsymbol{v}}_s^r = R_s \vec{\boldsymbol{i}}_s^r + L_s \frac{d\vec{\boldsymbol{i}}_s^r}{dt} + jL_s \omega_r \vec{\boldsymbol{i}}_s^r + j\psi_m \omega_r, \tag{4}$$

where $\vec{\boldsymbol{v}}_s^r = \vec{\boldsymbol{v}}_s e^{-j\theta_r}$, $\vec{\boldsymbol{i}}_s^r = \vec{\boldsymbol{i}}_s e^{-j\theta_r}$, and the superscript r denote rotor coordinates.

The stator equation (4) can be rewritten in d-q axis coordinates as follows:

$$\begin{aligned} v_d &= R_s i_d + L_d \frac{di_d}{dt} - L_q \omega_r i_q \\ v_q &= R_s i_q + L_q \frac{di_q}{dt} + L_d \omega_r i_d + \psi_m \omega_r \end{aligned}, \tag{5}$$

where L_d, L_q are the d-axis and q-axis inductances, i_d, i_q are the d-axis and q-axis stator currents, v_d, v_q are

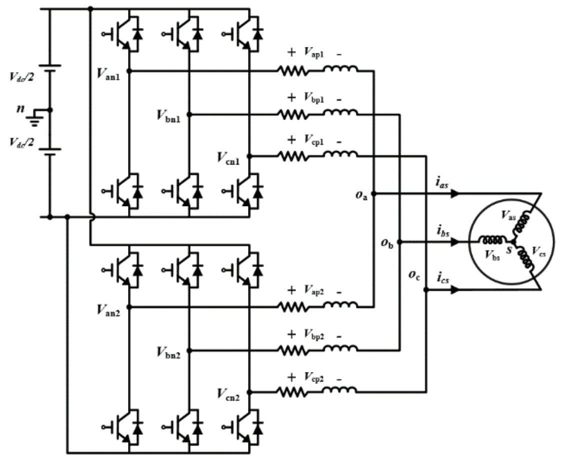

Fig. 2. Parallel inverters equivalent circuit for a motor drive system

the d-axis and q-axis stator voltages, respectively, and $\vec{v}_s^r = v_d + jv_q$ and $\vec{i}_s^r = i_d + ji_q$. The electric torque produced by the machine can be expressed as follows:

$$T_e = \frac{3}{2} p \left[\psi_m \cdot i_q + \left(L_d - L_q \right) i_d \cdot i_q \right], \tag{6}$$

where T_e is the electric torque and p denotes the number of pole pairs. The mechanical equation of the rotor is considered in (7),

$$J \frac{d\omega_m}{dt} = T_e - T_L, \tag{7}$$

where the coefficient J denotes the moment of inertia of the mechanical shaft, ω_m is the mechanical rotor speed, and T_L is the load torque of the machine.

2.3 Modeling of Parallel Inverters

Fig. 2 shows a parallel inverter circuit for driving a motor, including the pole voltage, phase voltage, and inductor output voltage of parallel inverters. For convenient analysis, it is assumed that the switches making up the parallel inverters are ideal and that the equivalent resistance of the output inductor in Fig. 2 is negligible. It is also assumed that the switches of each leg do not close at the same time, in order to prevent a DC-link short circuit. The switching state of each leg can be defined by the switching function S_i in (8). Here, "1" means that the upper switch is closed, and "0" means that the lower switch is closed.

$$S_i = \begin{cases} 1 & when\ S_i\ is\ closed \\ 0 & when\ S_i\ is\ open \end{cases} \tag{8}$$

From (8), the pole voltage of the inverter V_{inx} can be expressed by (9),

$$\begin{aligned} V_{inx} &= S_{ix} \cdot \frac{V_{dc}}{2} + \left(S_{ix} - 1 \right) \cdot \frac{V_{dc}}{2} \\ &= V_{dc} \left(S_{ix} - \frac{1}{2} \right) \end{aligned}, \tag{9}$$

where V_{dc} represents a DC-link voltage.

In Fig. 2, when KCL is applied to the node o_i connected in common to the output inductor and the motor, the following equation is satisfied:

$$i_{is1} + i_{is2} = i_{is}. \tag{10}$$

If the ratio of the output inductance to the d, q inductance of the IPMSM is defined as N, (11) can be obtained:

$$N = 3 \frac{L_{ipx}}{L_d + L_q}. \tag{11}$$

At this time, assuming that the switching state does not change during one sampling time, the sampling time is sufficiently small, and the electromotive force is constant, the output inductor voltage and the phase voltage of the motor can also be regarded as constant during that time. Therefore, the currents of the output inductor and the motor can be approximated by (12) and (13), respectively, using the inductor voltage equation:

$$i_{ix}\left(t_0 + T_s \right) \approx \frac{1}{L_{ipx}} \cdot V_{ipx} \cdot T_s + i_{ix}\left(t_0 \right), \tag{12}$$

$$i_{is}\left(t_0 + T_s \right) \approx \frac{1}{L_{is}} \cdot V_{is} \cdot T_s + i_{is}\left(t_0 \right), \tag{13}$$

where t_0 represents an arbitrary sampling time, T_s is one sampling time, L_{is} is each phase inductance of the motor, V_{ipx} is the output inductor voltage, and V_{is} represents the phase voltage of the motor.

By substituting (11), (12), and (13) into (10), the relationship between the output inductor voltage and the motor phase voltage can be obtained as (14):

$$V_{ip1} + V_{ip2} = N \cdot V_{is}, \tag{14}$$

where V_{ip1} represents the output inductor voltage of Inverter 1 and V_{ip2} represents the output inductor voltage of Inverter 2.

If KVL is applied to the virtual closed loop between the DC-link neutral point n and the motor neutral point s in Fig. 2, the inverter pole voltage V_{inx} is expressed as (15):

$$V_{inx} = V_{ipx} + V_{is} + V_{sn}, \tag{15}$$

where V_{sn} denotes the voltage between the virtual neutral point of the DC-link capacitor and the neutral point of the motor.

Table 1. The voltage vector of parallel inverters

Space Vector		Switching State	Space Vector	Switching State
Zero Vector	$\overrightarrow{V_0}$	[000] [000]	-	-
Active Vector	$\overrightarrow{V_1}$	[000] [100]	$\overrightarrow{V_2}$	[000] [110]
	$\overrightarrow{V_3}$	[000] [010]	$\overrightarrow{V_4}$	[000] [011]
	$\overrightarrow{V_5}$	[000] [001]	$\overrightarrow{V_6}$	[000] [101]
	$\overrightarrow{V_7}$	[100] [110]	$\overrightarrow{V_8}$	[010] [110]
	$\overrightarrow{V_9}$	[010] [011]	$\overrightarrow{V_{10}}$	[001] [011]
	$\overrightarrow{V_{11}}$	[001] [101]	$\overrightarrow{V_{12}}$	[100] [101]
	$\overrightarrow{V_{13}}$	[100] [100]	$\overrightarrow{V_{14}}$	[110] [110]
	$\overrightarrow{V_{15}}$	[010] [010]	$\overrightarrow{V_{16}}$	[011] [011]
	$\overrightarrow{V_{17}}$	[001] [001]	$\overrightarrow{V_{18}}$	[101] [101]

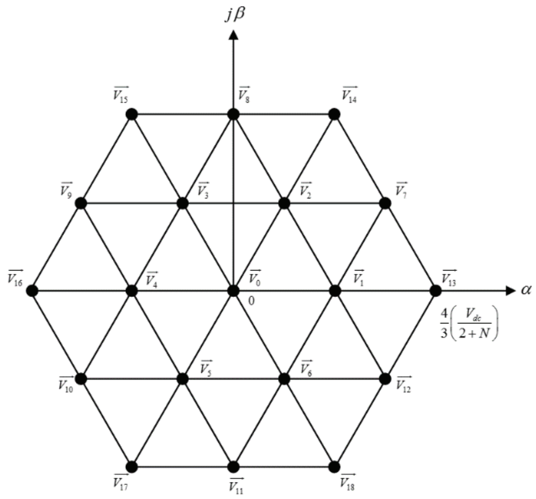

Fig. 3. The space voltage vector of parallel inverters

Assuming that the three-phase voltage of the motor is balanced, (16) can be obtained by summing the pole voltages of Inverter 1 and Inverter 2 according to (15):

$$V_{sn} = \frac{1}{6}\left(V_{an1} + V_{bn1} + V_{cn1} + V_{an2} + V_{bn2} + V_{cn2}\right). \qquad (16)$$

The motor phase voltages from (14) and (15) are as follows:

$$V_{is} = \frac{1}{(2+N)}\left(V_{in1} + V_{in2} - 2V_{sn}\right). \qquad (17)$$

The following equation is obtained by substituting (9) and (16) into (17), and finally, the phase voltage of the motor in the parallel inverters can be expressed as a switching function in (18),

$$V_{is} = \frac{V_{dc}}{(2+N)}\begin{Bmatrix} S_{i1} + S_{i2} \\ -\frac{1}{3}\left(S_{a1} + S_{b1} + S_{c1} + S_{a2} + S_{b2} + S_{c2}\right) \end{Bmatrix}. \qquad (18)$$

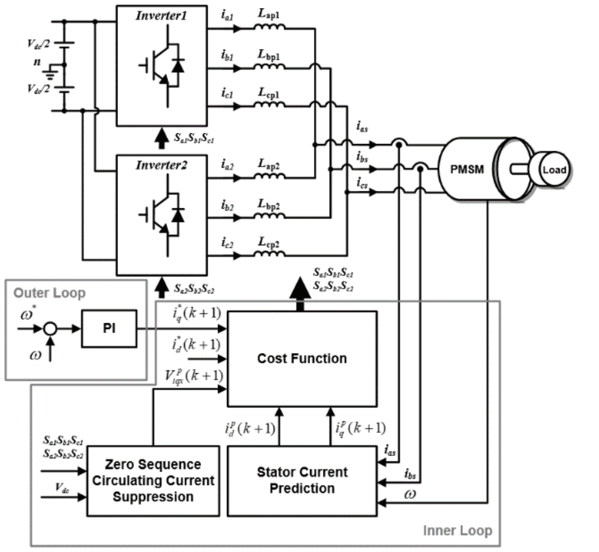

Fig. 4. Block diagram of the proposed control method for zero-sequence circulating current suppression

The space voltage vectors of 19 parallel inverters are listed in Table 1 and can be expressed by the Clarke coordinate transformation equation of (19) in the stationary reference frame, as shown in Fig. 3. The space voltage vector of the parallel inverters is composed of one zero vector and 18 effective vectors.

$$\begin{bmatrix} V_{\alpha s} \\ V_{\beta s} \end{bmatrix} = \frac{2}{3}\begin{bmatrix} 1 & -\frac{1}{2} & -\frac{1}{2} \\ 0 & \frac{\sqrt{3}}{2} & -\frac{\sqrt{3}}{2} \end{bmatrix}\begin{bmatrix} V_{as} \\ V_{bs} \\ V_{cs} \end{bmatrix} \qquad (19)$$

Here, $V_{\alpha s}$ and $V_{\beta s}$ represent the phase voltages of the motor transformed to the α -axis and β -axis in the stationary reference frames, respectively.

3. Proposed Method for Zero-Sequence Circulating Current Suppression

Fig. 4 shows a control block diagram of the parallel inverters based on MPC for driving IPMSM. In the proposed scheme, the control block diagram consists of a stator flux component and electromagnetic torque component controller based on MPC in the inner loop, and the speed controller, a traditional PI controller, in the outer loop. The internal controller is made up of three blocks. In the stator current prediction block, the stator current of the motor is sensed and expressed in the rotor reference frame aligned with the rotor flux axis, and then the stator current is predicted using the discrete time prediction model. In the zero-sequence circulating current suppression block, the output inductor voltage is predicted using the switching function relationship of the parallel inverters model derived in Section 2. In the cost function block, the predicted current and output inductor voltage according to the 19 switching states are applied to the cost function, and then the cost function values are compared with each other. Finally, the inverter voltage vector minimizing the cost function for the next sampling period k+1 is selected as the optimal switching state. Therefore, among the 19 voltage vectors, we can apply a voltage vector that suppresses the circulating current and supplies optimal current control to the parallel inverters.

3.1 Stator current prediction

The Euler approximation method is applied to the stator current differential term to predict the stator current after sampling time T_s as follows:

$$\frac{di}{dt} \approx \frac{i(k+1) - i(k)}{T_s}. \tag{20}$$

By substituting (20) into (5), the predicted stator current on the d-q rotor reference frame can be obtained as in (21) and (22).

$$i_d^p(k+1) = \left(1 - \frac{R_s T_s}{L_d}\right) i_d(k) + \frac{T_s \omega_r}{L_d} L_q i_q(k) + \frac{T_s}{L_d} v_d \tag{21}$$

$$i_q^p(k+1) = \left(1 - \frac{R_s T_s}{L_q}\right) i_q(k) - \frac{T_s \omega_r}{L_q}\left(L_d i_d(k) + \psi_m\right) + \frac{T_s}{L_q} v_q \tag{22}$$

where $i_d(k)$ and $i_q(k)$ denote the d-q current at the resent sampling time, and $i_d^p(k+1)$ and $i_q^p(k+1)$ represent the d-q current predicted at the next sampling period k+1. As shown in (21) and (22), it is possible to predict the stator current of the next period via the stator current, voltage, sampling time and motor parameters. Further, by applying (21) and (22) to the cost function, predictive current control can be performed for the motor drive.

3.2 Zero-Sequence Circulating Current Suppression

3.2.1 Proposed zero-sequence circulating current suppression method

Fig. 5 shows the equivalent circuit of the output inductor for any one phase. The current difference between Inverter 1 and Inverter 2 can be defined as in (23),

$$i_{iz} = i_{i1} - i_{i2}, \tag{23}$$

where i_{iz} is defined as the circulating current of the phase. In Fig. 5, it is assumed that the inductance value of the output inductor is equal to L_{ip}. The difference V_{ip} between the output inductor voltage of Inverter 1 and the output inductor voltage of Inverter 2 can be expressed by (24):

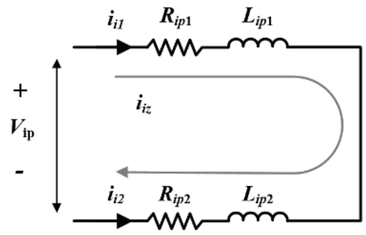

Fig. 5. The equivalent circuit of the output inductor of one phase

$$V_{ip} = L_{ip}\frac{di_{iz}}{dt} + R_{ip1} i_{i1} - R_{ip2} i_{i2}. \tag{24}$$

At this time, if the inverters are controlled so that becomes 0, it should satisfy both (25) and (26) simultaneously,

$$i_{iz} = i_{i1} - i_{i2} = const. \tag{25}$$

$$i_{i1} = \frac{R_{ip2}}{R_{ip1}} i_{i2}. \tag{26}$$

Assuming that the equivalent resistances R_{ip1} and R_{ip2} of the output inductor are the same in (26), finally, i_{i1} and i_{i2} become equal, and the circulating current i_{iz} is not generated. In other words, it can be seen that the circulating current can be suppressed by controlling V_{ip} at a minimum.

3.2.2 Modeling of output inductor voltage

The relationship in (15) between the output inductor voltage and the motor phase voltage can be rewritten as V_{ipx}, as shown in (27).

$$V_{ipx} = V_{inx} - \left(V_{is} + V_{sn}\right) \tag{27}$$

By substituting (9), (16), and (18) into (27), the output inductor voltage V_{ipx} can be obtained according to the DC-link voltage, inductance ratio, and the switching state of each phase.

$$\begin{aligned} V_{ipx} &= V_{dc}\left(S_{ix} - \frac{1}{2}\right) \\ &- \left(\begin{aligned} &\frac{V_{dc}}{(2+N)}\left[\begin{aligned} &S_{i1} + S_{i2} \\ &-\frac{1}{3}\left(S_{a1} + S_{b1} + S_{c1} + S_{a2} + S_{b2} + S_{c2}\right) \end{aligned}\right] \\ &+\frac{V_{dc}}{6}\left[S_{a1} + S_{b1} + S_{c1} + S_{a2} + S_{b2} + S_{c2} - 3\right] \end{aligned} \right) \end{aligned} \tag{28}$$

3.3 Cost function optimization

The cost function, including the circulating current suppression, is expressed as (29):

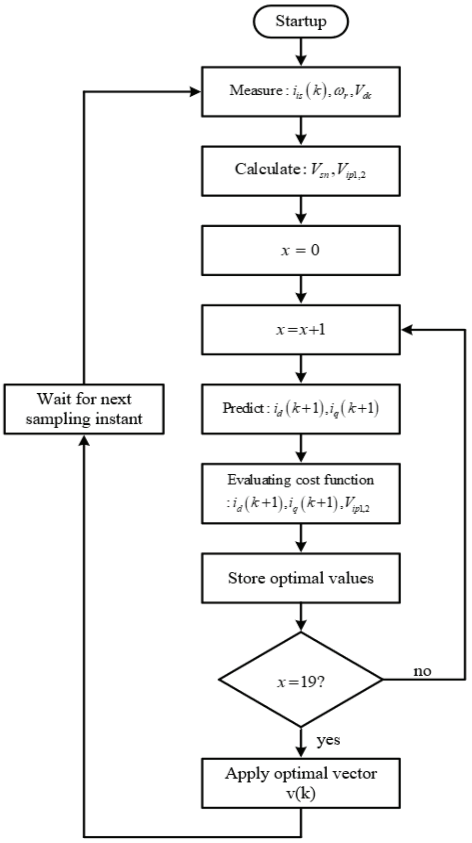

Fig. 6. The flowchart of the proposed method

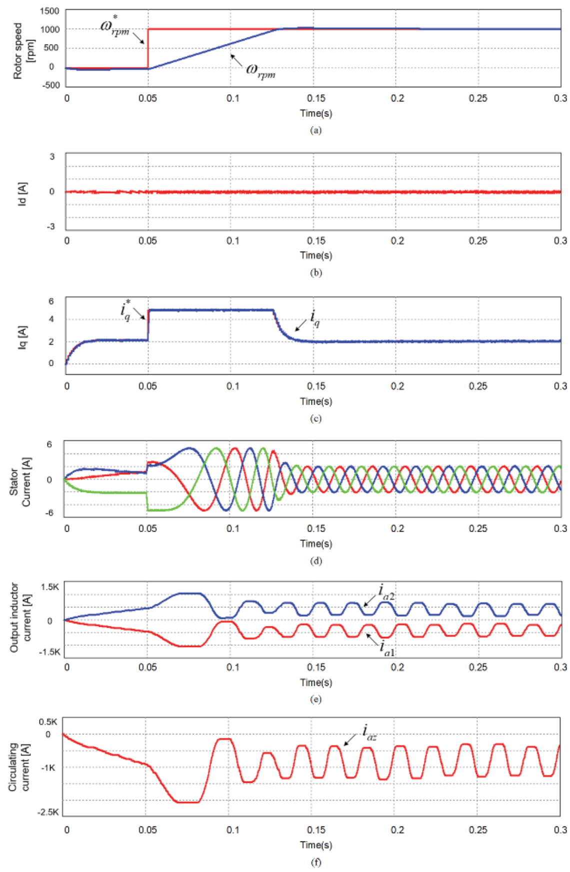

Fig. 7. Simulated waveforms without application of the proposed method in parallel inverters: (a) speed, (b) d-axis current, (c) q-axis current, (d) stator current, (e) output inductor current, and (f) circulating current

Table 2. Motor and control parameters

Parameter	Value	Unit
Pole pairs	3	-
d-axis inductance	11.5	mH
q-axis inductance	20	mH
Stator resistance	1.134	Ω
Permanent magnet flux linkage	0.109	Wb
Rated power	600	W
Rated speed	3600	rpm
DC-link voltage	100	V
Interphase inductor inductance	326	uH
Sampling time	66.7	us

$$g = \left| i_d^*(k+1) - i_d^p(k+1) \right| - \left| i_q^*(k+1) - i_q^p(k+1) \right| + \lambda \left| V_{ip1}^p(k+1) - V_{ip2}^p(k+1) \right| , \quad (29)$$

where $i_d^*(k+1)$, $i_q^*(k+1)$ are the reference currents in the rotor d-q reference frame, $V_{ip1}^p(k+1)$, $V_{ip2}^p(k+1)$ are the output inductor voltages of Inverters 1 and 2 predicted at the next sampling period k+1, g is the cost function, and λ is the weighting factor for circulating current suppression. In this paper, $i_d^*(k+1)$ is set to 0 and $i_q^*(k+1)$ is generated in the PI speed controller.

The cost function of (29) consists of the d-q axis stator current term for motor current control and the output inductor voltage term for circulating current control. In the rotor reference frame aligned with the rotor flux axis, the d-axis component of the stator current is proportional to the stator flux and the q-axis component is proportional to the electrical torque. Therefore, d-axis and q-axis current control is required to control the stator flux and torque component of the motor, so the term of the d-q axis stator current is included in the cost function. In addition, the inductor output voltage term to suppress the circulating current is further applied to the cost function. The cost function is expressed by the error between the reference value and the predicted value, and the voltage vector that minimizes the cost function is selected.

All possible voltage vectors are substituted into (29) to determine the minimum value of the cost function, and an optimal voltage vector that suppresses circulating current is applied to the parallel inverters. This enables the parallel inverters to operate with motor side current sensing alone. The proposed control method can be implemented in the following sequence as shown in Fig. 6.

As mentioned above, system nonlinearity and limited elements (circulating current suppression) can be included in the cost function of MPC, increasing flexibility and ease of application.

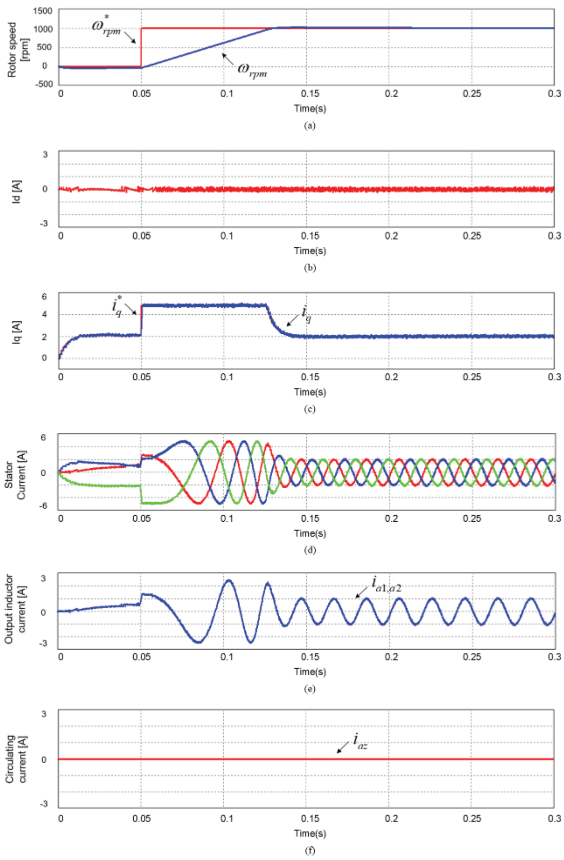

Fig. 8. Simulated waveforms in parallel inverters using the proposed method: (a) speed, (b) d-axis current, (c) q-axis current, (d) stator current, (e) output inductor current, and (f) circulating current

4. Simulation and Experimental Results

Simulations and experiments were conducted to verify the proposed model predictive control scheme used to suppress the circulating current of parallel inverters. The parameters of the motor and control system are listed in Table 2.

Fig. 7 shows the simulation waveform without application of the proposed model predictive control method, where the speed varies from 0 to 1000 rpm under 50% load conditions. As shown in Fig. 7(a), the actual speed ω_{rpm} follows the speed reference ω_{rpm}^* properly. From Figs. 7(b), (c), and (d), it can be seen that the d-axis and q-axis currents i_d and i_q also follow the reference currents i_d^* and i_q^*, respectively, and the three-phase stator current is balanced at the same time. However, as shown in Figs. 7(e) and (f), the output inductor currents i_{a1} and i_{a2} of Inverters 1 and 2, respectively, diverge, indicating the occurrence of a large circulating current i_{az} . Fig. 8 shows the waveform with application of the proposed model predictive control method under the same operating conditions. The speed and current are appropriately controlled via the proposed method, as shown in Figs. 8(a) through (d). In addition, as shown in Figs. 8(e) and (f), the circulating current i_{az} is also effectively suppressed.

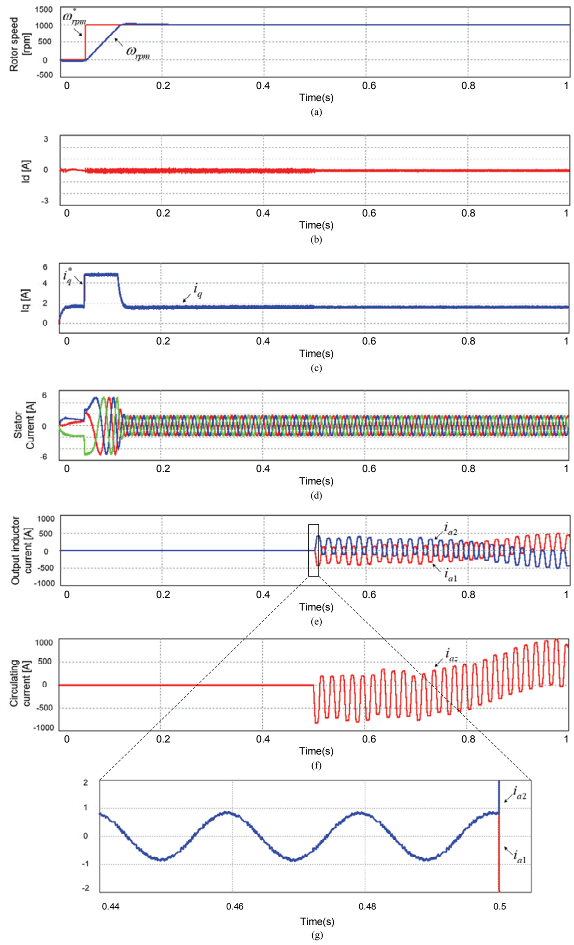

Fig. 9. Simulated waveforms initially with proposed method and without proposed method after 0.5s: (a) speed, (b) d-axis current, (c) q-axis current, (d) stator current, (e) output inductor current, (f) circulating current, and (g) zoomed output inductor current

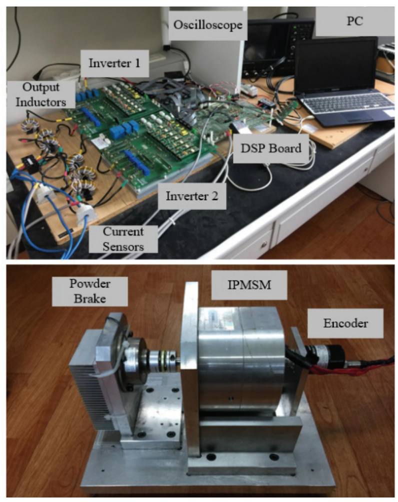

Fig. 10. Experimental setup

In order to clearly show the comparison about with and

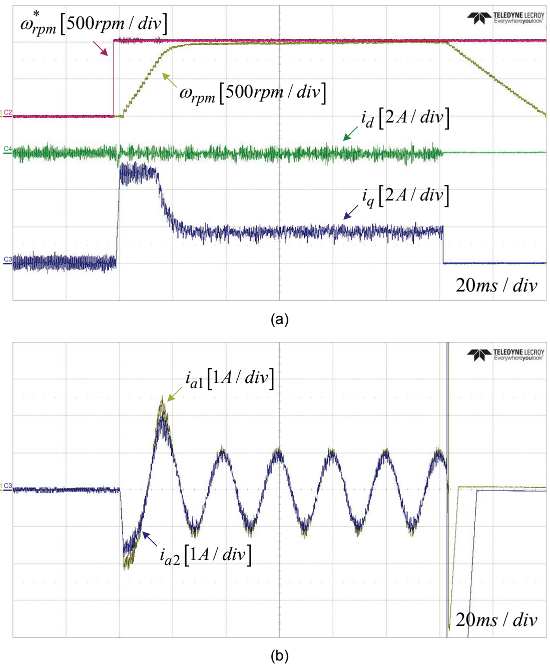

Fig. 11. Experimental results without application of the proposed method: (a) rotor speed, d-axis current, q-axis current, (b) output inductor currents

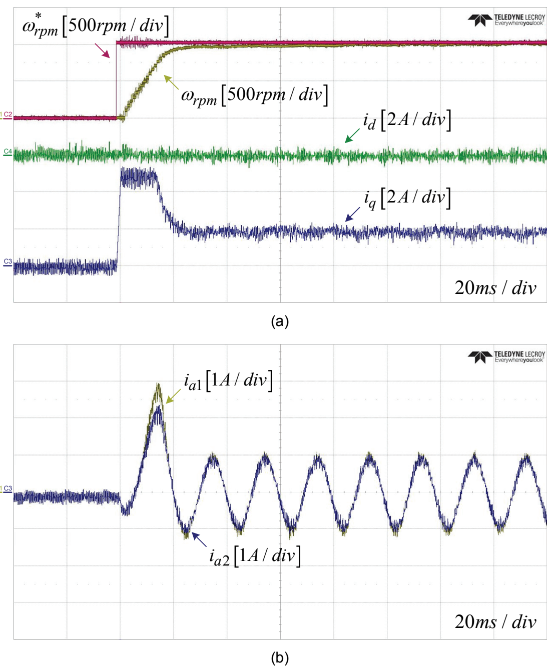

Fig. 12. Experimental results with application of the proposed method: (a) rotor speed, d-axis current, q-axis current, (b) output inductor currents

without the proposed method, Fig. 9 shows simulation waveforms of control mode change over. Initially, we set the weighting factor for circulating current control to 1 in the cost function of (29) and set the weighting factor to 0 in 0.5 second. As shown in Figs. 9(e), (f), (g), the output

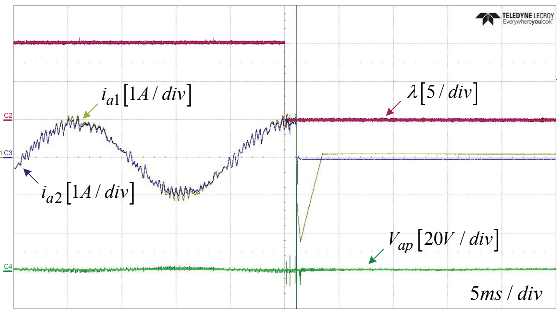

Fig. 13. Experimental results of the difference between the a-phase output inductor voltage of Inverter 1 and Inverter 2 without application of the proposed method

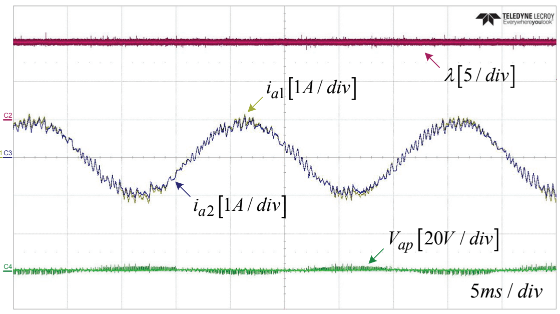

Fig. 14. Experimental results of the difference between the a-phase output inductor voltage of Inverter 1 and Inverter 2 with application of the proposed method

inductor currents i_{a1} and i_{a2} diverge after 0.5 seconds, and the circulating current is generated. In addition, the zoomed inductor current waveform in Fig. 9(g) also shows the detail situation of the current divergence.

Fig. 10 shows the prototype used in the experiment to verify the proposed method. Only two current sensors were used to measure the phase current of the motor without an additional current sensor in the output inductor, and the load torque was applied through the powder brake.

Figs. 11 and 12 show the waveforms from the start to the steady state, and the rotor speed command value, real rotor speed, d, q-axis current, and a-phase current of Inverter 1 and 2 at 50% load and 1000 rpm conditions. Figs. 11 (a), (b) show the experimental results when the proposed method is not used. Initially, the motor was driven by the proposed method and approximately 120ms after inputting the speed command value, the proposed method is no longer applied. The speed and current are well controlled in the beginning, but after 120ms, the output inductor current diverges from Inverter 1 and 2, causing a current fault and the speed decreases to zero. On the other hand, Figs. 12 (a), (b) show the experimental results when the proposed method is used. As shown in Fig. 12 (a), the speed and current are well controlled. Fig. 12 (b) shows the experimental result of the output inductor current with the application of the proposed method, where the two-phase inductor currents are controlled to be equal to each other, and the circulating current is effectively suppressed. Likewise, inductor currents in the b-phase and c-phase were also suppressed.

To show more the performance of the proposed method, Figs. 13 and 14 show the difference between the a-phase output inductor voltage of Inverter 1 and 2 with and without the proposed algorithm. If the weighting factor is changed from 10 to 0 as shown in Fig. 13, the output inductor voltage term is neglected in the cost function of (29), so the difference between the a-phase output inductor voltage of Inverter 1 and 2 is induced. Therefore, the output inductor current is diverging. On the other hand, when the weighing factor is kept at 10 as shown in Fig. 14, the proposed method controls the difference between the a-phase output inductor voltage of Inverter 1 and 2 to 0, which effectively suppresses the circulating current.

5. Conclusion

In this paper, we analyze and discuss the use of an MPC scheme for a parallel inverter-fed IPMSM drive. We derive the voltage vectors of the parallel inverters for accurate prediction and control of the stator flux and torque components. When the parallel inverters are driven via MPC, the voltage vector that does not generate the zero-sequence circulating current by sensing only the two-phase currents on the motor is selected using the cost function. This vector is then applied to the inverters. Finally, in the proposed method, a balanced three-phase stator current is achieved and the zero-sequence circulating current is suppressed. Simulation and experimental results are presented to verify the validity of the proposed method in a parallel inverter IPMSM drive system.

Acknowledgements

This work was supported by "Human Resources Program in Energy Technology" of the Korea Institute of Energy Technology Evaluation and Planning (KETEP), granted financial resource from the Ministry of Trade, Industry & Energy, Republic of Korea. (No. 20164010200860).

References

[1] S. Ogasawara, J. Takagaki, H. Akagi and A. Nabae, "A novel control scheme of a parallel current-controlled PWM inverter," *IEEE Transactions on Industry Applications*, vol. 28, pp. 1023-1030, September/October 1992.

[2] Y. Komatsuzaki, "Cross current control for parallel operating three phase inverter," *Power Electronics Specialists Conference, PESC '94 Record., 25th Annual IEEE*, vol. 2, pp. 943-950, June 1994.

[3] Y. Sato and T. Kataoka, "Simplified control strategy to improve AC input-current waveform of parallel-connected current-type PWM rectifiers," *IEE Proceedings - Electric Power Applications*, vol. 142, pp. 246-254, July 1995.

[4] Zhihong, Ye, D. Boroyevich, Jae-Young, Choi and F. C. Lee, "Control of circulating current in two parallel three-phase boost rectifiers," *IEEE Transactions on Power Electronics*, vol. 17, pp. 609-615, September 2002.

[5] F. Wang, Y. Wang, Q. Gao, C. Wang and Y. Liu, "A Control Strategy for Suppressing Circulating Currents in Parallel-Connected PMSM Drives with Individual DC Links," *IEEE Transactions on Power Electronics*, vol. 31, pp. 1680-1691, February 2016.

[6] Z. Zhang, A. Chen, X. Xing and C. Zhang, "A novel model predictive control algorithm to suppress the zero-sequence circulating currents for parallel three-phase voltage source inverters," *2016 IEEE Applied Power Electronics Conference and Exposition* (*APEC*), pp. 3465-3470, March 2016.

[7] Tsung-Po Chen, "Dual-Modulator Compensation Technique for Parallel Inverters Using Space-Vector Modulation," *IEEE Transactions on Industrial Electronics*, vol. 56, pp. 3004-3012, August 2009.

[8] B.M.H. Jassim, D.J. Atkinson, B. Zahawi, "Modular Current Sharing Control Scheme for Parallel-Connected Converters," *IEEE Transactions on Industrial Electronics*, vol. 62, pp. 887-897, February 2015.

[9] B. Wei, J. M. Guerrero, J. C. Vasquez, X. Guo, "A Circulating-Current Suppression Method for Parallel-Connected Voltage-Source Inverters With Common DC and AC Buses," *IEEE Transactions on Industrial Applications*, vol. 53, pp. 3758-3769, July/August 2017.

[10] P. Cortes, M. P. Kazmierkowski, R. M. Kennel, D. E. Quevedo and J. Rodriguez, "Predictive Control in Power Electronics and Drives," *IEEE Transactions on Industrial Electronics*, vol. 55, pp. 4312-4324, December 2008.

[11] Esteban J. Fuentes, Jose Rodriguez, Cesar Silva, Sergio Diaz, Daniel E. Quevedo, "Speed control of a permanent magnet synchronous motor using predictive current control," *Power Electronics and Motion Control Conference*, 2009. IPEMC '09. IEEE 6th International, pp. 390-395, May 2009.

[12] S. Vazquez, J. Rodriguez, M. Rivera, L. G. Franquelo and M. Norambuena, "Model Predictive Control for Power Converters and Drives: Advances and Trends," *IEEE Transactions on Industrial Electronics*, vol. 64, pp. 935-947, February 2017.

[13] G. A. Papafotiou, G. D. Demetriades and V. G. Agelidis, "Technology Readiness Assessment of Model Predictive Control in Medium- and High-

Voltage Power Electronics," *IEEE Transactions on Industrial Electronics*, vol. 63, pp. 5807-5815, September 2016.

[14] C. Bordons and C.Montero, "Basic principles of MPC for power converters: Bridging the gap between theory and practice," *IEEE Ind. Electron. Mag.*, vol. 9, no. 3, pp. 31-43, Sep. 2015.

[15] S. Vazquez et al., "Model predictive control: A review of its applications in power electronics," *IEEE Ind. Electron. Mag.*, vol. 8, no. 1, pp. 16-31, Mar. 2014.

[16] P. Karamanakos, T. Geyer, N. Oikonomou, F. D. Kieferndorf, and S. Manias, "Direct model predictive control: A review of strategies that achieve long prediction intervals for power electronics," *IEEE Ind. Electron. Mag.*, vol. 8, no. 1, pp. 32-43, Mar. 2014.

[17] J. Rodriguez et al., "State of the art of finite control set model predictive control in power electronics," *IEEE Trans. Ind. Informat.*, vol. 9, no. 2, pp. 1003-1016, May 2013.

Shin-Won Kang He received the B.S degree in electrical and control engineering from Hanyang University, Seoul, Korea, in 2012, where he is currently working toward the direct Ph.D. degree. His current research interests include model-predictive control for power converters and motor drives and wide-band gap devices.

Jae-Hwan Soh He received the B.S degree in electrical and control engineering from Hanyang University, Seoul, Korea, in 2012, where he is currently working toward the direct Ph.D. degree. His current research interests include high efficiency converter/inverter for high power density, wide-bandgap devices, and model-predictive control.

Rae-Young Kim He received the B.S. and M.S. degrees from Hanyang University, Seoul, Korea, in 1997 and 1999, respectively, and the Ph.D. degree from Virginia Polytechnic Institute and State University, Blacksburg, VA, USA, in 2009, all in electrical engineering. From 1999 to 2004, he was a Senior Researcher at the Hyosung Heavy Industry R&D Center, Seoul, Korea. In 2009, he was a Postdoctoral Researcher at National Semiconductor Corporation, Santa Clara, CA, USA, involved in a smart home energy management system. In 2016, he was a Visiting Scholar with the Center for Power Electronics Systems (CPES), Virginia Polytechnic Institute and State University, Blacksburg. Since 2010, he has been with Hanyang University, where he is currently an Assistant Professor in the Department of Electrical and Biomedical Engineering. His research interests include modeling and control of distributed power converter systems, soft-switching techniques, energy management systems in microgrid applications, modular power converter for renewable energies and motor drive systems. Dr. Kim was a recipient of the 2007 First Prize Paper Award from the IEEE IAS.